Path Integral Approach to the Dynamic Casimir Effect with Fluctuating Boundaries

Ramin Golestanian
Institute for Advanced Studies in Basic Sciences, Zanjan 45195-159, Iran

Mehran Kardar
Department of Physics, Massachusetts Institute of Technology, Cambridge, MA 02139

(February 9, 2008)

A path integral formulation is developed for the *dynamic* Casimir effect. It allows us to study small deformations in *space and time* of the perfectly reflecting (conducting) boundaries of a cavity. The mechanical response of the intervening vacuum is calculated to linear order in the frequency–wavevector plane, using which a plethora of interesting phenomena can be studied. For a single corrugated plate we find a correction to mass at low frequencies, and an effective shear viscosity at high frequencies that are both anisotropic. The anisotropy is set by the wavevector of the corrugation. For two plates, the mass renormalization is modified by a function of the ratio between the separation of the plates and the wave-length of corrugations. The dissipation rate is not modified for frequencies below the lowest optical mode of the cavity, and there is a resonant dissipation for *all frequencies* greater than that. In this regime, a divergence in the response function implies that such high frequency deformation modes of the cavity can not be excited by any macroscopic external forces. This phenomenon is intimately related to resonant particle creation. For particular examples of two corrugated plates that are stationary, or moving uniformly in the lateral directions, Josephson-like effects are observed. For capillary waves on the surface of mercury a renormalization to surface tension, and sound velocity is obtained.

I. INTRODUCTION AND SUMMARY

The Casimir effect [1–5] is a surprising phenomenon in which quantum fluctuations of the electromagnetic field in the vacuum, subject to the boundary conditions imposed by two conducting plates of area A and separation H, lead to an attractive force between them, given by

$$F_{\rm static}(H) = -\frac{\pi^2}{240} \times \hbar c \frac{A}{H^4}. \tag{1}$$

This force, which provides a direct link between quantum field theory and the macroscopic world, has been measured experimentally (using a torsion pendulum) between a gold plate, and a gold plated sphere, to the accuracy of within %5 [6]. Related fluctuation-induced phenomena occur in various areas of physics ranging from cosmology to statistical mechanics of phase transitions [2,4].

Since the pioneering work of Casimir, various modifications to the standard boundary conditions have been studied. One generalization, relevant to experimental measurements of the force, is to introduce deformations (roughness) of the surfaces. For example, in Ref. [7] a multiple scattering approach is used to compute the interactions for arbitrary geometry in a perturbation series in the curvature. In another phenomenological approach, introduced in Ref. [9], small deviations from plane parallel geometry are treated by using an additive summation of van der Waals–type pair-wise potentials. The former method is difficult to implement, while the latter is not always reliable due to the additivity assumption [5].

New phenomena emerge for moving boundaries in the generalization to the *dynamic Casimir effect* [10–19]. The creation of photons by moving mirrors was first obtained by Moore [10] for a 1 dimensional cavity. Fulling and Davis [11] found a corresponding force proportional to the third time derivative of the mirror displacement. Their methods specifically make use of the conformal symmetries of the 1+1 dimensional space time, and hence are not applicable for the more realistic case of 1+3 dimensions [20].

Another approach to the dynamic Casimir effect starts with the fluctuations in the radiation pressure on a plate [13,14]. The fluctuation–dissipation theorem is then used to obtain the mechanical response function, whose imaginary part gives the dissipation in response to motion. This method does not suffer from the causality problems of earlier approaches [20], and can be applied to all dimensions. For example, the force in 1+3 dimensional space-time depends on the fifth time derivative of the displacement. Several other approaches have focused on the emission of photons

by a vibrating cavity [15–17]. This is generally too small to be experimentally detectable [18,22]; the most promising set-up is the resonant production of photons when the mirrors vibrate at the optical resonance frequency of the cavity [18]. More recently, the radiation due to vacuum fluctuations of a collapsing bubble has been proposed as a possible explanation for the intriguing phenomenon of sonoluminescense [21,22]. A good review of the topic including more extensive references can be found in Ref. [23].

A number of authors have further discussed to notion of *frictional forces*: Using conformal methods in 1+1 dimensions, Ref. [24] finds a friction term

$$F_{\rm friction}(H) = \alpha\, F_{\rm static}(H)\, \left(\frac{\dot{H}}{c}\right)^2 , \tag{2}$$

for slowly moving boundaries, where α is a numerical constant that only depends on dimensionality. The additional factor of $(v/c)^2$ would make detection of this force yet more difficult. There are a few attempts to calculate forces (in higher dimensions) for walls that move *laterally*, i.e. parallel to each other [25–27]: It is found that boundaries that are not ideal conductors, experience a friction as if the plates are moving in a viscous fluid. The friction has a complicated dependence on the frequency dependent resistivity of the plates, and vanishes in the cases of ideal (nondissipating) conductors or dielectrics. The "dissipation" mechanism for this "friction" is by inducing eddy currents in the nonideal conductors, and thus distinct from the Casimir effect.

In this paper we present a path integral formulation, applicable to all dimensions, for the problem of perfectly reflecting mirrors that undergo small dynamic deformations. Although the original Casimir problem with parallel plates can be tackled with such a path integral approach (see Appendix A), it is much easier to solve by the standard operator method, followed by expansions in modes appropriate to the specified geometry and boundary conditions. However, if one wishes to study the effect of deformations of either static (fixed roughness) or dynamic nature, the standard method is hardly tractable [9,28]. In contrast, the path integral method is much better suited to handling deformations. The only limitation of the method is that it provides the result as a perturbative expansion in powers of the ratio between the deformation field and the average separation of the plates. In the present context, a great advantage of this method is that it does not make any distinction between "time" and "space" coordinates provided that appropriate Wick rotations are performed. Consequently, one can consider time dependent boundary conditions with no additional complications.

Using this procedure, we calculate the mechanical response function in the frequency–wavevector domain. It is defined as the ratio between the induced force and the deformation field, in the linear regime. From the response function we extract a plethora of interesting results, some of which we list here for the specific example of lateral vibrations of uniaxially corrugated plates:

- **(1)** A single plate with corrugations of wavenumber $\mathbf{k}$, vibrating at frequencies $\omega \ll ck$, obtains *anisotropic* corrections to its mass. Thus the effective mass of a plate depends on its shape!
- **(2)** For $\omega \gg ck$, there is dissipation due to a frequency dependent anisotropic shear viscosity, i.e. a type of 'friction' in the vacuum.
- **(3)** A second plate at a separation H modifies the mass renormalization by a function of kH, but does not change the dissipation for frequencies $\omega^2 < (ck)^2 + (\pi c/H)^2$.
- **(4)** For all frequencies higher than this first optical normal mode of the cavity, the mechanical response is infinite, implying that such modes can not be excited by any finite external force. This is intimately connected to the resonant particle creation reported in the literature [15,18]. It is also an example of radiation from neutral bodies, a purely quantum effect.
- **(5)** A phase angle θ between two similarly corrugated plates results in Josephson–like effects: A static force proportional to $\sin(\theta)$, and an oscillating force for a uniform relative velocity.
- **(6)** There is a (minute) correction to the velocity of capillary waves on the surface of mercury due to a small change in its surface tension.

The rest of the paper is organized as follows. In Sec.II we develop the formalism to calculate the effective action for time dependent small deformation fields. In Sec.III the behavior of the mechanical response functions are examined in the frequency–wavevector domain. We discuss the important special case of lateral oscillations of rough plates in Sec.IV, and Sec.V gives the conclusions of the paper, and suggests avenues for future explorations. In Appendix A the path integral method is applied to the standard Casimir effect due to the electromagnetic field, while some details of the calculations are included in Appendix B.

II. PATH INTEGRAL FORMULATION OF THE DYNAMIC CASIMIR EFFECT

In this section we introduce a quantization method for a field, subject to boundary conditions on surfaces which undergo dynamic shape fluctuations. Although one can tackle the gauge invariant electromagnetic vector field by this formalism (see Appendix A), we use for simplicity the "scalar electrodynamics" model used most commonly in the literature [10,28]. We consider a scalar field described by the classical action ($c = 1$)

$$S = \frac{1}{2}\int \mathrm{d}^d X\ \partial_\mu \phi(X)\partial_\mu \phi(X), \tag{3}$$

where summation over $\mu = 1, \cdots, d$ in a d dimensional space-time is understood, and we have made a Wick rotation by introducing the imaginary time variable $X^d = it$. We want to quantize the field ϕ subject to the constraint that it vanishes on a set of manifolds (objects) embedded in space-time. The manifolds are described by functions $X^\mu = X^\mu_\alpha(y_\alpha)$; a D_α-dimensional manifold embedded in d-dimensional space is parametrized by $y_\alpha \equiv (y^1_\alpha, \cdots, y^{D_\alpha}_\alpha)$. Following Ref. [8], the partition function of the system is written as

$$\begin{aligned}\mathcal{Z} &= \frac{1}{\mathcal{Z}_0}\int \mathcal{D}\phi(X) \prod_{\alpha=1}^{n}\prod_{y_\alpha} \delta\left(\phi\left(X_\alpha(y_\alpha)\right)\right)\ \exp\left\{-\frac{1}{\hbar}S[\phi]\right\}, \\ &= \frac{1}{\mathcal{Z}_0}\int \mathcal{D}\phi(X) \prod_{\alpha=1}^{n}\mathcal{D}\psi_\alpha(y_\alpha)\ \exp\left\{-\frac{1}{\hbar}S[\phi] + i\sum_\alpha \int \mathrm{d}y_\alpha \sqrt{g_\alpha}\ \psi_\alpha(y_\alpha)\phi\left(X_\alpha(y_\alpha)\right)\right\},\end{aligned} \tag{4}$$

where $\mathcal{Z}_0$ is the partition function for the system with no boundaries, and g_α is the determinant of the induced metric on the α'th manifold [29],

$$g_{\alpha,ij} = \frac{\partial X^\mu_\alpha}{\partial y^i_\alpha}\frac{\partial X^\mu_\alpha}{\partial y^j_\alpha}, \tag{5}$$

required to make the integration measure over the manifolds reparametrization invariant.

The integration over the field ϕ can be performed, and the resulting expression for the partition function is

$$\mathcal{Z} = \int \prod_\alpha \mathcal{D}\psi_\alpha(y_\alpha) \exp\left\{-S_1[\psi_\alpha(y_\alpha)]\right\}, \tag{6}$$

where

$$S_1[\psi] \equiv \psi^T M \psi = \sum_{\alpha,\beta}\int \mathrm{d}y_\alpha \sqrt{g_\alpha}\mathrm{d}y_\beta\sqrt{g_\beta}\psi_\alpha(y_\alpha)G^d(X_\alpha(y_\alpha) - X_\beta(y_\beta))\psi_\beta(y_\beta), \tag{7}$$

and $G^d(X - X') = (-\partial_\mu\partial_\mu)^{-1}_{XX'}$. Integrating over the Gaussian fields $\{\psi_\alpha\}$ gives the final result of

$$\ln \mathcal{Z} = -\frac{1}{2}\ln\det\{M(X_\alpha(y_\alpha))\}. \tag{8}$$

We next focus on the specific example of two D (space-time) dimensional surfaces in $d = D + 1$ space-time with average separation H, and small deformations. The surfaces are thus parametrized by $X_1(\mathbf{x}) = (\mathbf{x}, h_1(\mathbf{x}))$ and $X_2(\mathbf{x}) = (\mathbf{x}, H + h_2(\mathbf{x}))$, where $h_1(\mathbf{x})$ and $h_2(\mathbf{x})$ are the deformations. One can read off the matrix M from Eq.(7) as

$$M(\mathbf{x},\mathbf{y}) = \begin{bmatrix} \sqrt{g_1(\mathbf{x})}\sqrt{g_1(\mathbf{y})}\ G^d(\mathbf{x}-\mathbf{y}, h_1(\mathbf{x}) - h_1(\mathbf{y})) & \sqrt{g_2(\mathbf{x})}\sqrt{g_1(\mathbf{y})}\ G^d(\mathbf{x}-\mathbf{y}, H + h_2(\mathbf{x}) - h_1(\mathbf{y})) \\ \sqrt{g_1(\mathbf{x})}\sqrt{g_2(\mathbf{y})}\ G^d(\mathbf{x}-\mathbf{y}, H + h_2(\mathbf{y}) - h_1(\mathbf{x})) & \sqrt{g_2(\mathbf{x})}\sqrt{g_2(\mathbf{y})}\ G^d(\mathbf{x}-\mathbf{y}, h_2(\mathbf{x}) - h_2(\mathbf{y})) \end{bmatrix}, \tag{9}$$

in which $\sqrt{g_\alpha(\mathbf{x})} = \sqrt{1 + (\nabla h_\alpha)^2}$ where the gradient is with respect to the plane (space-time) coordinates (see Eq.(5)). Following Ref. [8], we perform a perturbative expansion of the matrix in terms of the deformation fields, as

$$M(\mathbf{x},\mathbf{y}) = M_0(\mathbf{x},\mathbf{y}) + \delta M(\mathbf{x},\mathbf{y}). \tag{10}$$

The matrix

$$M_0(\mathbf{x},\mathbf{y}) = \begin{bmatrix} G^d(\mathbf{x}-\mathbf{y}, 0) & G^d(\mathbf{x}-\mathbf{y}, H) \\ G^d(\mathbf{x}-\mathbf{y}, H) & G^d(\mathbf{x}-\mathbf{y}, 0) \end{bmatrix}, \tag{11}$$

describes two flat plates and is only a function of the differences of the coordinates. Hence it can be transformed using a Fourier basis into

$$M_0(\mathbf{p},\mathbf{q}) = \begin{bmatrix} G^d(\mathbf{p}) & G^d(\mathbf{p},H) \\ G^d(\mathbf{p},H) & G^d(\mathbf{p}) \end{bmatrix} (2\pi)^D \delta^D(\mathbf{p}+\mathbf{q}), \tag{12}$$

where

$$\begin{aligned} G^d(\mathbf{p}) &= \int \mathrm{d}^D\mathbf{x}\; G^d(\mathbf{x},0)\; \mathrm{e}^{i\mathbf{p}\cdot\mathbf{x}}, \\ G^d(\mathbf{p},H) &= \int \mathrm{d}^D\mathbf{x}\; G^d(\mathbf{x},H)\; \mathrm{e}^{i\mathbf{p}\cdot\mathbf{x}}, \end{aligned} \tag{13}$$

are the Fourier-transformed Green's functions.

The part of the partition function that depends on the deformation fields can be written as $\ln \mathcal{Z}_h = -\frac{1}{2}\ln\det\{1 + M_0^{-1}\delta M\}$. Expanding everything in powers of $h(\mathbf{x})$, and keeping only up to second order terms, we obtain (for details of the calculations see Appendix B)

$$\begin{aligned} \ln \mathcal{Z}_h = &\frac{1}{2}\int \mathrm{d}^D\mathbf{x}\mathrm{d}^D\mathbf{y}\; K(\mathbf{x}-\mathbf{y})\; [h_1(\mathbf{x})h_1(\mathbf{y}) + h_2(\mathbf{x})h_2(\mathbf{y})] \\ &- \frac{1}{2}\int \mathrm{d}^D\mathbf{x}\mathrm{d}^D\mathbf{y}\; Q(\mathbf{x}-\mathbf{y})\; [h_1(\mathbf{x})h_2(\mathbf{y}) + h_1(\mathbf{y})h_2(\mathbf{x})]\,. \end{aligned} \tag{14}$$

The kernels in the above equation are defined as

$$\begin{aligned} K(\mathbf{x}) &= \partial_z^2 G(\mathbf{x},0)F_1(\mathbf{x}) + F_1(\mathbf{x})F_5(\mathbf{x}) + F_4(\mathbf{x})F_6(\mathbf{x}), \\ Q(\mathbf{x}) &= \partial_z^2 G(\mathbf{x},H)F_4(\mathbf{x}) + F_2(\mathbf{x})^2 + F_3(\mathbf{x})^2, \end{aligned} \tag{15}$$

where

$$\begin{aligned} F_1(\mathbf{x}) &= \int \frac{d^D\mathbf{p}}{(2\pi)^D}\frac{G^d(\mathbf{p})}{\mathcal{N}(\mathbf{p})}\; \mathrm{e}^{i\mathbf{p}\cdot\mathbf{x}}, \\ F_2(\mathbf{x}) &= \int \frac{d^D\mathbf{p}}{(2\pi)^D}\frac{G^d(\mathbf{p})}{\mathcal{N}(\mathbf{p})}\;\frac{\partial G^d(\mathbf{p},H)}{\partial H}\; \mathrm{e}^{i\mathbf{p}\cdot\mathbf{x}}, \\ F_3(\mathbf{x}) &= \int \frac{d^D\mathbf{p}}{(2\pi)^D}\frac{G^d(\mathbf{p},H)}{\mathcal{N}(\mathbf{p})}\;\frac{\partial G^d(\mathbf{p},H)}{\partial H}\; \mathrm{e}^{i\mathbf{p}\cdot\mathbf{x}}, \\ F_4(\mathbf{x}) &= \int \frac{d^D\mathbf{p}}{(2\pi)^D}\frac{G^d(\mathbf{p},H)}{\mathcal{N}(\mathbf{p})}\; \mathrm{e}^{i\mathbf{p}\cdot\mathbf{x}}, \\ F_5(\mathbf{x}) &= \int \frac{d^D\mathbf{p}}{(2\pi)^D}\frac{G^d(\mathbf{p})}{\mathcal{N}(\mathbf{p})}\;\left(\frac{\partial G^d(\mathbf{p},H)}{\partial H}\right)^2\; \mathrm{e}^{i\mathbf{p}\cdot\mathbf{x}}, \\ F_6(\mathbf{x}) &= \int \frac{d^D\mathbf{p}}{(2\pi)^D}\frac{G^d(\mathbf{p},H)}{\mathcal{N}(\mathbf{p})}\;\left(\frac{\partial G^d(\mathbf{p},H)}{\partial H}\right)^2\; \mathrm{e}^{i\mathbf{p}\cdot\mathbf{x}}, \end{aligned} \tag{16}$$

and

$$\mathcal{N}(\mathbf{p}) = \left[G^d(\mathbf{p})\right]^2 - \left[G^d(\mathbf{p},H)\right]^2. \tag{17}$$

We now focus on the case of interest in the Casimir problem which corresponds to $d = 4$ and $D = 3$. The Green's functions can be calculated from the definition following Eq.(7), and using Eqs.(13) as

$$\begin{aligned} G^4(\mathbf{p}) &= \frac{1}{2p}, \\ G^4(\mathbf{p},H) &= \frac{1}{2p}\; \mathrm{e}^{-pH}, \\ \partial_z^2 G^4(\mathbf{x},0) &= -\frac{1}{2\pi^2}\;\frac{1}{x^4}, \\ \partial_z^2 G^4(\mathbf{x},H) &= -\frac{1}{2\pi^2}\;\frac{x^2-3H^2}{(x^2+H^2)^3}. \end{aligned} \tag{18}$$

To obtain the behavior due to the time dependence of shape fluctuations of the surfaces, we rotate back to "real" time variables, changing Eq.(14) to

$$\begin{aligned}\ln \mathcal{Z}_h = & -\frac{1}{2}\int \mathrm{d}t\mathrm{d}t'\mathrm{d}^2x\mathrm{d}^2y\; K(x-y,it-it')\;\left[h_1(x,t)h_1(y,t')+h_2(x,t)h_2(y,t')\right] \\ & +\frac{1}{2}\int \mathrm{d}t\mathrm{d}t'\mathrm{d}^2x\mathrm{d}^2y\; Q(x-y,it-it')\;\left[h_1(x,t)h_2(y,t')+h_1(y,t')h_2(x,t)\right].\end{aligned} \tag{19}$$

One can diagonalize the above expression using the Fourier transformations

$$h_\alpha(x,t)=\int \frac{\mathrm{d}\omega\mathrm{d}^2q}{(2\pi)^3}\;\mathrm{e}^{-i\omega t+iq\cdot x}\;h_\alpha(q,\omega), \tag{20}$$

for the fields. The corresponding transformations for the kernels result in

$$\begin{aligned}\mathcal{K}(q,\omega) &= \int \mathrm{d}t\mathrm{d}^2x\;\mathrm{e}^{-i\omega t+iq\cdot x}K(x,it) \\ &= -i\int_{-\infty}^{\infty}\mathrm{d}\tau\int \mathrm{d}^2x\;\mathrm{e}^{-\omega\tau+iq\cdot x}K\left(\sqrt{x^2+\tau^2}\right) \\ &\equiv -i\;A_+(q,\omega),\end{aligned} \tag{21}$$

and

$$\begin{aligned}\mathcal{Q}(q,\omega) &= \int \mathrm{d}t\mathrm{d}^2x\;\mathrm{e}^{-i\omega t+iq\cdot x}Q(x,it) \\ &= -i\int_{-\infty}^{\infty}\mathrm{d}\tau\int \mathrm{d}^2x\;\mathrm{e}^{-\omega\tau+iq\cdot x}Q\left(\sqrt{x^2+\tau^2}\right) \\ &\equiv -i\;A_-(q,\omega),\end{aligned} \tag{22}$$

where we have performed a rotation of the integration contours from it to τ. The symmetric appearance of the argument $\sqrt{x^2+\tau^2}$ in Eqs.(21) and (22) is due to the underlying Lorentz invariance of the theory. Finally, the resulting expression for the effective action, defined via $\ln\mathcal{Z}=iS_{\rm eff}/\hbar$, reads

$$\begin{aligned}S_{\rm eff}=\frac{\hbar c}{2}\int\frac{\mathrm{d}\omega\mathrm{d}^2q}{(2\pi)^3}\;\{&A_+(q,\omega)\left(|h_1(q,\omega)|^2+|h_2(q,\omega)|^2\right) \\ &-A_-(q,\omega)\left(h_1(q,\omega)h_2(-q,-\omega)+h_1(-q,-\omega)h_2(q,\omega)\right)\}.\end{aligned} \tag{23}$$

III. ANALYTIC STRUCTURE OF THE RESPONSE KERNELS

The kernels $A_\pm(q,\omega)$ are closely related to the mechanical response of the system. By substituting the expressions of Eq.(18) in Eqs.(15-17) and (21,22), after some manipulations, one obtains

$$A_\pm(q,\omega)=\frac{\pi^2}{64H^5}\int_{-\infty}^{+\infty}\mathrm{d}s\left(\frac{\sin\left[2\sqrt{q^2-\omega^2/c^2}Hs/\pi\right]}{2\sqrt{q^2-\omega^2/c^2}Hs/\pi}\right)g_\pm(s),\quad \text{for } \omega<cq. \tag{24}$$

For $\omega>cq$, the result is obtained by *analytic continuation* of the above. The need for such analytic continuation is a distinction between Minkowski and Euclidean spaces, and did not occur in Ref. [8]. In Eq.(24),

$$g_\pm(s)=\left(\frac{1}{s^3}\pm\frac{\cosh s}{\sinh^3 s}\right)^2+\frac{\sinh^2 s}{\cosh^6 s}\pm 2s\frac{\sinh s}{\cosh^3 s}\left[\frac{s^2-3\pi^2/4}{(s^2+\pi^2/4)^2}\right], \tag{25}$$

are two functions of the dimensionless parameter s, and upper and lower cut-offs for the space-time are understood in case of divergences. It can be seen that the kernels are functions of the separation H, but depend on $\mathbf{q}$ and ω only through the combination $Q^2=q^2-\omega^2/c^2$. Rather than elaborating on the closed forms of the kernels, we shall describe their behavior in various regions of the parameter space.

The kernels can be calculated exactly for a single mirror. It is simpler to take the $H \to \infty$ limit in the original Eqs.(15-18), and (21,22). Additional manipulations lead to $A_-^\infty(q,\omega) = 0$, and

$$A_+^\infty(q,\omega) = \begin{cases} -\frac{1}{360\pi^2 c^5}(c^2q^2 - \omega^2)^{5/2} & \text{for } \omega < cq, \\ i\frac{\mathrm{sgn}(\omega)}{360\pi^2 c^5}(\omega^2 - c^2q^2)^{5/2} & \text{for } \omega > cq, \end{cases} \tag{26}$$

where $\mathrm{sgn}(\omega)$ is the sign function. While the effective action and the corresponding response are real for $Q^2 > 0$, they become purely imaginary for $Q^2 < 0$. The analytic continuation to this regime is not unique. However, if we require causality for the response, we are led to the choice in which the imaginary part is an odd function, leading to the inclusion of the sign function in the above formula. An imaginary response function signals dissipation of energy [13], presumably by creation of photons as shown in the next section [17]. For the special case of $q = 0$, Eq.(26) agrees with the results obtained previously [13] for flat mirrors. (Note that Ref. [13] considers the electromagnetic field rather than a scalar field, accounting for the discrepancy in the numerical prefactor. We have also done the same calculations in 1+1 dimensions and have reproduced the result of Refs. [11,12], who also use scalar fields, with the correct coefficient.)

In the presence of a second plate (i.e. for finite H), the situation is more complicated. For $Q^2 > 0$, we can examine the behavior of the integrand in Eq.(24) and find that the kernels are *real* and *finite* in this regime. However, for $Q^2 < 0$ the situation is different. Applying contour integration, we can transform the integral in Eq.(24) to the form

$$\mathcal{I} = 2\pi i \sum \text{residues} - \mathcal{CI}, \tag{27}$$

where $\mathcal{CI}$ is the contribution from the semicircle at infinity. The residues can be easily shown to be finite and real, and add to up to a finite and well behaved sum. Examining the contributions from the semicircle at infinity, we find terms with both real and imaginary parts, that generically behave as $\mathcal{CI} \sim \exp[(K-2)L/H]/[K(L/H)^3]$, with $K = 2Q'H/\pi$, $Q' = iQ$. L is the radius of the semicircle, presumably corresponding to an upper cut-off in space-time. Now we can see that in the limit $L \to \infty$, the situation drastically changes at $K = 2$. While $\mathcal{CI}$ vanishes for $K \leq 2$, it diverges with both real and imaginary parts for $K > 2$, where the inequality is understood in its strict sense.

To summarize, we can subdivide the parameter space of the kernels into three different regions, as depicted in Fig. 1. In region I ($Q^2 > 0$ for any H), the kernels are finite and real, and hence there is no dissipation. In region IIa where $-\pi^2/H^2 \leq Q^2 < 0$, the H-independent part of A_+ is imaginary, while the H-dependent parts of both kernels are real and finite. (This is also the case at the boundary $Q^2 = -\pi^2/H^2$.) The dissipation in this regime is simply the sum of what would have been observed if the individual plates were decoupled, and unrelated to the separation H. By contrast, in region IIb where $Q^2 < -\pi^2/H^2$, both kernels diverge with infinite real and imaginary parts. This H-dependent divergence extends all the way to the negative Q^2 axis, where it is switched off by a $1/H^5$ prefactor. Note that some care is necessary in the order of limits for $(L, H) \to \infty$.

Divergence of the kernels might be argued to signal a breakdown of the perturbation theory. However, one should note that the exponential divergence of the kernels is an essential singularity that can not be "cured" by standard renormalization techniques. It is in fact an artifact of the unphysical assumption of perfect reflectivity for the mirrors at *all* frequencies. Any natural frequency cut-off for the reflectivity of the mirror will round off this divergence [17], leading to a finite mechanical response. In other words, the imperfection in reflectivity at low frequencies provides a leakage mechanism for the cavity that stops the resonant energy build-up. Exponential creation of photons (with observation time) for perfectly reflecting boundaries has also been reported in the literature for the case of a one dimensional cavity [16], using a completely different approach.

IV. CORRUGATED PLATES

We now concentrate on a concrete example, and examine the lateral vibrations of surfaces with fixed (time independent) roughness, such as two corrugated plates. We assume that the first plate undergoes a lateral motion described by $\mathbf{r}(t)$, while the second plate is stationary. The deformations of the plates are thus described by $h_1(\mathbf{x},t) = h_1(\mathbf{x} - \mathbf{r}(t))$ and $h_2(\mathbf{x},t) = h_2(\mathbf{x})$. The lateral force exerted on the first plate is obtained from $f_i(t) = \delta S_{\text{eff}}/\delta r_i(t)$. Using Eq.(23), and within linear response, this is given by

$$f_i(\omega) = \chi_{ij}(\omega)\, r_j(\omega) + f_i^0(\omega), \tag{28}$$

where the "mechanical response tensor" is

$$\chi_{ij}(\omega) = \hbar c \int \frac{\mathrm{d}^2 q}{(2\pi)^2}\, q_i q_j \left\{ \left[A_+(q,\omega) - A_+(q,0)\right]\ |h_1(\mathbf{q})|^2 + \frac{1}{2} A_-(q,0)\left(h_1(\mathbf{q})h_2(-\mathbf{q}) + h_1(-\mathbf{q})h_2(\mathbf{q})\right)\right\}, \tag{29}$$

and there is a residual (static) force

$$f_i^0(\omega) = -\frac{\hbar c}{2}\, 2\pi\delta(\omega)\ \int \frac{\mathrm{d}^2 q}{(2\pi)^2}\, i q_i A_-(q,0)\left(h_1(\mathbf{q})h_2(-\mathbf{q}) - h_1(-\mathbf{q})h_2(\mathbf{q})\right). \tag{30}$$

We can calculate the dissipation rate

$$\begin{aligned} P &= \lim_{T\to\infty} \frac{1}{T} \int_{-T/2}^{T/2} \mathrm{d}t\ \dot{\mathbf{r}}(t)\cdot\mathbf{f}(t), \\ &= \frac{1}{T}\int_{-\infty}^{+\infty} \frac{\mathrm{d}\omega}{2\pi}\, i\omega\ \chi_{ij}(\omega)\ r_i(-\omega) r_j(\omega), \\ &= -\frac{1}{T}\int_{-\infty}^{+\infty} \frac{\mathrm{d}\omega}{2\pi}\, \omega\ \mathrm{Im}\chi_{ij}(\omega)\ r_i(-\omega) r_j(\omega), \end{aligned} \tag{31}$$

in which we have used the fact that real (imaginary) part of a response function is an even (odd) function of frequency. Using the above formulas, we can predict various interesting effects for corrugated plates, that appear due to quantum fluctuations of vacuum.

A. Single plate phenomena

For a single corrugated plate, whose deformation is defined as $h(\mathbf{x}) = d\cos\mathbf{k}\cdot\mathbf{x}$, one can easily calculate the response tensor using the explicit formulas in Eq.(26). In the low-frequency limit, i.e. when $\omega \ll ck$, we can expand the result in powers of ω. This gives $\chi_{ij} = \delta m_{ij}\omega^2 + O(\omega^4)$, where $\delta m_{ij} = A\hbar d^2 k^3 k_i k_j/(288\pi^2 c)$, and can be regarded as corrections to the mass of the plate [30]. (Cut-off dependent mass corrections also appear, as in Ref. [23].) Note that these mass corrections are *anisotropic*, with

$$\begin{aligned} \delta m_\parallel &= A\hbar k^5 d^2/(288\pi^2 c), \\ \delta m_\perp &= 0. \end{aligned} \tag{32}$$

Parallel and perpendicular components are defined with respect to $\mathbf{k}$, and A denotes the area of the plates. The mass correction is proportional to $\hbar$, and hence inherently very small. For example, if we have a macroscopic sample with $d \approx \lambda = 2\pi/k \approx 1$mm, density $\approx 15\mathrm{gr/cm}^3$, and thickness $t \approx 1$ mm, we find $\delta m/m \sim 10^{-34}$. Even for deformations of a microscopic sample of atomic dimensions (close to the limits of the applicability of our continuum representations of the boundaries), $\delta m/m$ can only be reduced to around 10^{-10}. While the actual changes in mass are immeasurably small, the hope is that its *anisotropy* may be more accessible, say by comparing oscillation frequencies of a corrugated plate in two orthogonal directions.

For $\omega \gg ck$, which is the high-frequency limit, the response function is imaginary, and we can define a frequency dependent effective shear viscosity by $\chi_{ij}(\omega) = -i\omega\eta_{ij}(\omega)$. This viscosity is also anisotropic, with

$$\begin{aligned} \eta_\parallel(\omega) &= \hbar A k^2 d^2 \omega^4/(720\pi^2 c^4), \\ \eta_\perp(\omega) &= 0. \end{aligned} \tag{33}$$

Note that in 1+3 dimensions the dissipation is proportional to the fifth time derivative of displacement, and there is no dissipation for a uniformly accelerating plate. However, a freely oscillating plate will undergo a damping of its motion. The characteristic decay time for a plate of mass M is $\tau \approx 2M/\eta$. For the macroscopic plate of the previous paragraph, vibrating at a frequency of $\omega \approx 2ck$ (in the 10^{12}Hz range), the decay time is enormous, $\tau \sim 10^{18}$s. However, since the decay time scales as the fifth power of the dimension, it can be reduced to 10^{-12}s, for plates of order of 10 atoms. However, the required frequencies in this case (in the 10^{18}Hz range) are very large. Also note that for the linearized forms to remain valid in this high frequency regime, we must require very small amplitudes, so that the typical velocities involved $v \sim r_0\omega$, are smaller than the speed of light. These difficulties can be somewhat overcome by considering resonant dissipation in the presence of a second plate.

B. Double plate phenomena

With two plates at an average distance H, the results are qualitatively the same for frequencies less than the natural resonance of the resulting cavity. There is a renormalization of mass in region I, and dissipation appears in region IIa, of Fig. 1. However, the mass renormalization at low frequencies ($\omega \ll ck$) is now a function of both k and H, with a crossover from the single plate behavior for $kH \sim 1$. In the limit of $kH \ll 1$, we obtain

$$\begin{aligned} \delta m_{\parallel} &= \hbar A B k^2 d^2/48cH^3, \\ \delta m_{\perp} &= 0, \end{aligned} \tag{34}$$

with

$$B = \int_0^\infty \mathrm{d}s \; s^2 \; \left[-\frac{4}{s^6} + g_+(s) \right] \approx -0.452448. \tag{35}$$

Compared to the single plate, there is an enhancement by a factor of $(kH)^{-3}$ in $\delta m_{\parallel}$. The effective dissipation in region IIa is simply the sum of those due to individual plates, and contains no H dependence.

There are additional interesting phenomena resulting from resonances. We find that both real and imaginary parts of $A_{\pm}(q,\omega)$, diverge for $\omega^2/c^2 > q^2 + \pi^2/H^2$, that corresponds to region IIb of Fig. 1. In the example of corrugated plates, we replace q by k to obtain a continuous spectrum of frequencies with diverging dissipation. (Note that the imaginary part of the response function gives the dissipation.) Related effects have been reported in the literature for 1+1 dimensions [15–18], but occuring at a *discrete* set of frequencies $\omega_n = n\pi c/H$ with integer $n \geq 2$. These resonances occur when the frequency of the external perturbation matches the natural normal modes of the cavity, thus exciting quanta of such modes. In one space dimension, these modes are characterized by a discrete set of wavevectors that are integer multiples of π/H. The restriction to $n \geq 2$ is a consequence of quantum electrodynamics being a 'free' theory (quadratic action): only two-photon states can be excited subject to conservation of energy. Thus the sum of the frequencies of the two photons should add up to the external frequency [17].

In higher dimensions, the appropriate parameter is the combination $\omega^2/c^2 - q^2$. From the perspective of the excited photons, conservation of momentum requires that their two momenta add up to q, while energy conservation restricts the sum of their frequencies to ω. The in-plane momentum q, introduces a continuous degree of freedom: the resonance condition can now be satisfied for a continuous spectrum, in analogy with optical resonators. In Ref. [17], the lowest resonance frequency is found to be $2\pi c/H$ which seems to contradict our prediction. However, the absence of $\omega_1 = \pi c/H$ in 1+1 D is due to a vanishing prefactor [17], which is also present in our calculations. However, in exploring the continuous frequency spectrum in higher dimensions, this single point is easily bypassed, and there is a divergence for all frequencies satisfying $\omega^2/c^2 > q^2 + \pi^2/H^2$, where the inequality holds in its strict sense.

Resonant dissipation has profound consequences for motion of plates. It implies that due to quantum fluctuations of vacuum, *components of motion with frequencies in the range of divergences cannot be generated by any finite external force*! The imaginary parts of the kernels are proportional to the total number of excited photons [17]. Exciting these degrees of motion must be accompanied by the generation of an infinite number of photons; requiring an infinite amount of energy, and thus impossible. However, as pointed out in Ref. [17], the divergence is rounded off by assuming finite reflectivity and transmissivity for the mirrors. Hence, in practice, the restriction is softened and controlled by the degree of ideality of the mirrors in the frequency region of interest.

C. Josephson-like effects

Consider two plates corrugated at the same wavelength, and separated at a distance H, whose deformations are described by $h_1(\mathbf{x},t) = d_1 \; \cos[\mathbf{k}\cdot(\mathbf{x}-\mathbf{r}(t))]$ and $h_2(\mathbf{x},t) = d_2 \; \cos[\mathbf{k}\cdot\mathbf{x}]$. For the case of uniform motion of the plate, namely, $\mathbf{r}(t) = \mathbf{v}\,t + \mathbf{r}_0$, we can find the full expression for the lateral force as

$$\mathbf{f}(t) = \frac{\delta S_{\rm eff}}{\delta \mathbf{r}(t)} = \frac{\hbar c A}{2} A_-(k,0)\mathbf{k} d_1 d_2 \sin[\mathbf{k}\cdot\mathbf{r}(t)]. \tag{36}$$

While in previous expressions we performed a expansion to linear order in $\mathbf{r}(t)$, in Eq.(36) the complete expression is calculated using the time translational invaraince of a uniformly moving object. For two stationary plates ($\mathbf{v} = 0$) with a phase mismatch of $\alpha = \mathbf{k}\cdot\mathbf{r}_0$, there is a (time independent) lateral force

$$\mathbf{F}_{dc} = \frac{\hbar c A}{2} A_-(k,0)\mathbf{k} d_1 d_2 \sin\alpha, \tag{37}$$

which tends to keep the plates 180 degrees out of phase, i.e. mirror symmetric with respect to their mid-plane. This should be regarded as a correction to the static Casimir force due to the deformations of the plates. The dependence on the sine of the phase mismatch is reminiscent of the DC Josephson current in superconductor junctions, the force playing a role analogous to the current. (The amplitudes d_1 and d_2 are similar to the wave functions in SIS junctions.) Note that we could have equally well obtained this result using the constant term in Eq.(30).

For uniform motion, there is an analog for the AC Josephson effect, with velocity (the variable conjugate to force) playing the role of voltage. Setting $\mathbf{r}_0 = 0$, we find

$$\mathbf{F}_{ac} = \frac{\hbar c A}{2} A_-(k,0)\mathbf{k} d_1 d_2 \sin[(\mathbf{k}\cdot\mathbf{v})\ t], \tag{38}$$

where $A_-(k,0) = 1/H^5\ g(kH)$, with g a (dimensionless) slowly varying function of its argument. Note that the force oscillates at a frequency $\omega = \mathbf{k}\cdot\mathbf{v}$. Actually both effects are a consequence of the attractive nature of the Casimir force. It would be difficult to separate them from similar forces resulting from say, van der Waals attractions. One difference with (non-retarded) van der Waals force is in the power-law fall-off. Another potential difference with additive attractive interactions may be in the angular dependence of a static force. Such a difference in angular dependence due to the non-additive nature of thermal fluctuation-induced forces is discussed in Refs. [31,5] for two rods on a membrane. It is also likely to occur if we examine two rod-shaped deformations on the two plates in the Casimir geometry.

D. Capillary waves

In addition to solid corrugated plates, we can examine deformations of fluid surfaces. For example, consider the capillary waves on the surface of mercury, with a conducting plate placed at a separation H above the surface. The low frequency–wavevector expansion of the kernel due to quantum fluctuations in the intervening vacuum starts with quadratic forms q^2 and ω^2. These terms result in corrections to the (surface) mass density by $\delta\rho = \hbar B/48cH^3$, and to the surface tension by $\delta\sigma = \hbar cB/48H^3$ (B is the numerical constant calculated in Eq.(35)). The latter correction is larger by a factor of $(c/c_s)^2$, and changes the velocity c_s, of capillary waves by $\delta c_s/c_s^0 = \hbar cB/96\sigma H^3$, where σ is the bare surface tension of mercury. Taking $H \sim 1$mm and $\sigma \sim 500$ dynes/cm, we find another very small correction of $\delta c_s/c_s^0 \sim 10^{-19}$.

V. CONCLUSIONS AND OUTLOOK

In conclusion, we have developed a path integral formulation for the study of quantum fluctuations in a cavity with dynamically deforming boundaries. As opposed to previous emphasis on spectra of emitted radiation, we focus on the mechanical response of the vacuum from which we extract a variety of interesting mechanical effects. Most of the predicted dynamic Casimir phenomena, while quite intriguing theoretically, appear to be beyond the reach of current experiment: the most promising candidates are the anisotropy in mass, and resonant dissipation. A major difficulty is the necessity of exciting deformation modes of macroscopic objects in the 10^{12}Hz or higher frequency range. However, as the static Casimir effect seems more amenable to current experiments [6], it would be interesting to test the non-additive nature of this force for plates with rod-shaped deformations.

The path integral method is quite versatile: It is better suited to treating deformed boundaries than other techniques, such as that of Ref. [19]. Moreover, unlike other approaches [32], it provides the dispersive part of the response, as well as its dissipative part. Furthermore, we can envision a number of future extensions based on this formalism, some of which are listed below:

1. It is worthwhile to repeat the calculations for electromagnetic gauge fields. While we expect the above results to remain qualitatively unchanged, the vector nature of EM field, as well its gauge symmetry, may lead to novel additional phenomena. The transversality of photons in vacuum, as well differences between transverse electric (TE) and transverse magnetic (TM) modes, are two examples of the difference with scalar field, and may be important when considering the spectrum of emitted radiation (see below).

2. There have been some efforts to calculate the spectrum of radiation emitted from a single fluctuating mirror, or by a cavity with fluctuating walls [17,22]. Our formalism allows calculations in the more realistic case of 3+1

dimensional undulating walls. (Presumably, it is simpler to excite surface deformations of the boundaries at high frequencies, rather than rigidly oscillating the wall as a whole.) Radiation spectra can be obtained from two-point correlation functions which may be calculated by extending the methods of this paper. Hopefully, the angular distribution of the spectrum will provide signatures that can help in the experimental detection of such weak radiation.

3. New issues can be probed by extending the calculation to the next order in the deformation fields. For example, new dissipative terms may arise at the second order, resulting in a 'viscosity' proportional to the velocity-squared as in Eq.(2).

4. As in Ref. [8], it is possible to examine other geometries such as fluctuating 1 and 2 dimensional manifolds, corresponding respectively to world-lines of a point particle and a wire in space-time. We can then use our techniques to calculate the dynamic Casimir forces involved for fluctuating wires, and mutual interactions between moving particles, wires, and surfaces.

5. Dielectric superlattices are artificial media with nontrivial optical properties [33]. Because of the dielectric contrast in photonic crystals, they are excellent candidates for Casimir effects. In particular, dimensional arguments suggest that a photonic crystal with lattice spacing λ, will receive a density enhancement (presumably anisotropic) of the order of $\hbar/(c\lambda^4)$. While this is at best many orders of magnitude smaller than a typical density, it is none-the-less interesting to calculate the associated corrections to the mass tensor. It is more promising to examine the coupling of the vibrations of such superlattices to their optimal properties. In particular, do mechanical deformations (phonons) modify the optical function of a photonic crystal, due to quantum fluctuations of the vacuum?

6. An important generalization is to replace the assumption of perfectly metallic walls with boundary conditions that describe more realistic dielectric functions.

ACKNOWLEDGMENTS

RG acknowledges many helpful discussions with M.R.H. Khajehpour, B. Mashhoon, S. Randjbar-Daemi, and Y. Sobouti, and support from the Institute for Advanced Studies in Basic Sciences, Gava Zang, Zanjan, Iran. MK is supported by the NSF grant DMR-93-03667.

APPENDIX A: PATH INTEGRAL METHOD FOR THE ELECTROMAGNETIC FIELD

In this Appendix we introduce a path integral method for the standard static Casimir effect due to quantum fluctuations of the electromagnetic (EM) field. We start with the action

$$S_0 = -\frac{1}{4}\int \mathrm{d}^4X\sqrt{-g}\; g^{\mu\alpha}g^{\nu\beta}F_{\mu\nu}F_{\alpha\beta}, \tag{A1}$$

where $F_{\mu\nu} = \partial_\mu A_\nu - \partial_\nu A_\mu$, and $A_\mu = (A_0, -\mathbf{A})$ is the vector potential. We have introduced the constant (space-time independent) metric as a source, to enable calculation of the integral over the stress-energy tensor [34], as

$$\left.\frac{\partial S}{\partial g^{\mu\nu}}\right|_{\eta^{\mu\nu}} = \frac{1}{2}\int \mathrm{d}^4X\; T_{\mu\nu}(X), \tag{A2}$$

and $\eta^{\mu\nu} = \mathrm{diag}(-1,1,1,1)$ is the flat space-time metric.

We then take two perfectly conducting parallel plates separated a distance H along the z-direction. The boundary condition subject to which we have to quantize the theory is that the transverse electric field should vanish on the plates [2]. We should also treat the gauge freedom of the action by adopting a proper gauge fixing procedure. One can show that a possible proper quantization is achieved by considering the following expression for the generating function [35]

$$Z(g) = \lim_{\beta\to 0}\frac{1}{Z_0}\int \mathcal{D}A(X)\prod_{i,\alpha=1}^{2}\prod_{y_\alpha}\delta\left(\partial_0 A_i(X_\alpha(y_\alpha)) - \partial_i A_0(X_\alpha(y_\alpha))\right)\; \mathrm{e}^{\frac{i}{\hbar}S_\beta[A]}, \tag{A3}$$

where

$$S_\beta \equiv S_0[A] - \frac{\hbar}{2\beta}\int \mathrm{d}^4X\sqrt{-g}\,(g^{\mu\nu}\partial_\mu A_\nu)^2 \tag{A4}$$
$$= \int \mathrm{d}^4X\sqrt{-g}\left[\frac{1}{2}A_\mu\left(g^{\mu\nu}g^{\alpha\beta}\partial_\alpha\partial_\beta - g^{\mu\alpha}g^{\nu\beta}\partial_\alpha\partial_\beta(1-\frac{\hbar}{\beta})\right)A_\nu\right].$$

Now one can easily calculate the average value for energy using

$$-2i\hbar\left.\frac{\partial \ln Z(g)}{\partial g^{00}}\right|_{\eta^{\mu\nu}} = \int \mathrm{d}^4X\ \langle T_{00}(X)\rangle \tag{A5}$$
$$= AT\ \mathcal{E},$$

where A is the area of the plates, T is the overall time interval, and $\mathcal{E}$ is the Casimir energy. We now represent the delta-functions using Lagrange multiplier fields, as

$$Z(g) = \lim_{\beta\to 0}\frac{1}{Z_0}\int \mathcal{D}A(X)\prod_{i,\alpha=1}^{2}\mathcal{D}\psi_{i,\alpha}(y_\alpha)\ \exp\left\{\frac{i}{\hbar}S_\beta[A] + i\sum_{i,\alpha}\int \mathrm{d}y_\alpha\ \psi_{i,\alpha}(y_\alpha)\left(\partial_0 A_i(X_\alpha(y_\alpha)) - \partial_i A_0(X_\alpha(y_\alpha))\right)\right\}. \tag{A6}$$

Performing the integration over the gauge field, yields

$$Z(g) = \lim_{\beta\to 0}\frac{1}{Z_0}\int \prod_{i,\alpha=1}^{2}\mathcal{D}\psi_{i,\alpha}(y_\alpha)\ \exp\{-S[\psi_{i,\alpha}(y_\alpha)]\}, \tag{A7}$$

in which

$$S[\psi] = \psi^T M\psi = \sum_{\alpha,\beta}\int \mathrm{d}y_\alpha \mathrm{d}y_\beta\ [\partial_i\psi_{i,\alpha}(y_\alpha)G_{00}(X_\alpha(y_\alpha) - X_\beta(y_\beta))\partial_j\psi_{j,\alpha}(y_\alpha) \tag{A8}$$
$$+\partial_0\psi_{i,\alpha}(y_\alpha)G_{ij}(X_\alpha(y_\alpha) - X_\beta(y_\beta))\partial_0\psi_{j,\alpha}(y_\alpha)$$
$$-2\partial_0\psi_{i,\alpha}(y_\alpha)G_{0i}(X_\alpha(y_\alpha) - X_\beta(y_\beta))\partial_j\psi_{j,\alpha}(y_\alpha)],$$

and the matrix Green's functions satisfy

$$-i\left[g^{\mu\nu}g^{\alpha\beta}\partial_\alpha\partial_\beta - \left(1-\frac{\hbar}{\beta}\right)g^{\mu\alpha}g^{\nu\beta}\partial_\alpha\partial_\beta\right]G_{\nu\lambda}(X-X') = \delta^\mu_\lambda\delta^4(X-X'). \tag{A9}$$

The geometry of two parallel flat plates at a separation H is implemented using the embeddings $X_1(\mathbf{x},t) = (t,\mathbf{x},0)$, and $X_2(\mathbf{x},t) = (t,\mathbf{x},H)$. Then we can read off the matrix M from Eq.(A8). In Fourier space, it is diagonal and reads

$$M(p,q) = (2\pi)^3\delta^3(p+q)\ \left(p_ip_jM_{00} + p_0^2M_{ij} + p_0p_iM_{0j} + p_0p_jM_{0i}\right), \tag{A10}$$

in which

$$M_{\mu\nu} = \begin{bmatrix} G_{\mu\nu}(p,0) & G_{\mu\nu}(p,H) \\ G_{\mu\nu}(p,H) & G_{\mu\nu}(p,0)\end{bmatrix}, \tag{A11}$$

and

$$G_{\mu\nu}(p,H) = \int \mathrm{d}t\mathrm{d}^2\mathbf{x}\ G_{\mu\nu}(t,\mathbf{x},H)\ \mathrm{e}^{i\mathbf{p}\cdot\mathbf{x}-ip_0t}. \tag{A12}$$

Having found the matrix M, we can calculate the generating function from

$$\ln Z(g) = -\frac{1}{2}\ln\det\{M\}. \tag{A13}$$

To this end, we only need to determine the matrix Green's functions from Eq.(A9), which in momentum space are given by

$$G_{\nu\lambda}(P) = \frac{-i}{g^{\alpha\beta}P_\alpha P_\beta}\left[g_{\nu\lambda} + \left(\frac{\beta}{\hbar} - 1\right)\frac{P_\nu P_\lambda}{g^{\alpha\beta}P_\alpha P_\beta}\right], \tag{A14}$$

where P_ν is the four-momentum. At this point we can set $\beta = 0$, which implements the (Lorentz) gauge choice without any difficulty.

To simplify our calculations, we take the specific form $g^{\mu\nu} = \mathrm{diag}(g^{00}, 1, 1, 1)$ for the metric. This is sufficient for our purposes, as we are only need variations with respect to g^{00} to obtain the average energy. Inserting the matrix Green's functions from Eq.(A14), in Eqs.(A10-A12), we obtain after some manipulations,

$$M(p,q) = (2\pi)^3\delta^3(p+q)\left[-i\left(\frac{p_i p_j}{g^{00}} + p_0^2\delta_{ij}\right)\right] \otimes \begin{bmatrix} I(g^{00},p,0) & I(g^{00},p,H) \\ I(g^{00},p,H) & I(g^{00},p,0) \end{bmatrix}, \tag{A15}$$

where

$$I(g^{00},p,H) = \frac{\exp[-H(g^{00}p_0^2 + \mathbf{p}^2)^{1/2}]}{2(g^{00}p_0^2 + \mathbf{p}^2)^{1/2}}. \tag{A16}$$

We can next calculate the determinant to get

$$\ln Z(g) = -AT\int \frac{\mathrm{d}^3 p}{(2\pi)^3}\ \ln\left(1 - \exp\left[-2H(g^{00}p_0^2 + \mathbf{p}^2)^{1/2}\right]\right). \tag{A17}$$

Finally, we use Eq.(A5), and obtain

$$\mathcal{E} = -\frac{\pi^2}{720}\frac{\hbar c}{H^3}, \tag{A18}$$

which is the well known result for the Casimir energy [1].

APPENDIX B: PERTURBATION AROUND FLAT PLATES

In this Appendix we present the details of the calculations that lead to Eq.(14). We follow the steps and notations in the Appendix of Ref. [8]. We also generalize this work by including deformations of the second plate, and by using an invariant measure for integrations over the manifolds. We also note that the final result of Eq.(14), corrects some mistakes that appeared in Ref. [8]. To find δM we expand the square roots, as well as the Green's functions in Eq.(9) up to second order in the deformation

$$G^d(\mathbf{x}-\mathbf{y}, h_{1,2}(\mathbf{x}) - h_{1,2}(\mathbf{y})) = G^d(\mathbf{x}-\mathbf{y},0) + \frac{1}{2}\partial_z^2 G^d(\mathbf{x}-\mathbf{y},0)[h_{1,2}(\mathbf{x}) - h_{1,2}(\mathbf{y})]^2, \tag{B1}$$

$$\begin{aligned} G^d(\mathbf{x}-\mathbf{y}, H + h_2(\mathbf{x}) - h_1(\mathbf{y})) &= G^d(\mathbf{x}-\mathbf{y},H) + \partial_z G^d(\mathbf{x}-\mathbf{y},H)(h_2(\mathbf{x}) - h_1(\mathbf{y})) \\ &+ \frac{1}{2}\partial_z^2 G^d(\mathbf{x}-\mathbf{y},H)[h_2(\mathbf{x}) - h_1(\mathbf{y})]^2. \end{aligned} \tag{B2}$$

After Fourier transformation one obtains (see Eq.(10))

$$\delta M(\mathbf{p},\mathbf{q}) = \begin{bmatrix} B_1(\mathbf{p},\mathbf{q}) & A(\mathbf{p},\mathbf{q}) \\ A(\mathbf{q},\mathbf{p}) & B_2(\mathbf{p},\mathbf{q}) \end{bmatrix}, \tag{B3}$$

where

$$\begin{aligned} A(\mathbf{p},\mathbf{q}) = \int \mathrm{d}^D\mathbf{x}\mathrm{d}^D\mathbf{y}\ \mathrm{e}^{i\mathbf{p}\cdot\mathbf{x}+i\mathbf{q}\cdot\mathbf{y}}\Big\{&\frac{1}{2}G^d(\mathbf{x}-\mathbf{y},H)\left[(\nabla h_1(\mathbf{x}))^2 + (\nabla h_2(\mathbf{y}))^2\right] \\ &+\partial_z G^d(\mathbf{x}-\mathbf{y},H)(h_2(\mathbf{y}) - h_1(\mathbf{x})) \\ &+\frac{1}{2}\partial_z^2 G^d(\mathbf{x}-\mathbf{y},H)[h_2(\mathbf{y}) - h_1(\mathbf{x})]^2\Big\}, \end{aligned} \tag{B4}$$

$$\begin{aligned} B_{1,2}(\mathbf{p},\mathbf{q}) = \int \mathrm{d}^D\mathbf{x}\mathrm{d}^D\mathbf{y}\ \mathrm{e}^{i\mathbf{p}\cdot\mathbf{x}+i\mathbf{q}\cdot\mathbf{y}}\Big\{&\frac{1}{2}G^d(\mathbf{x}-\mathbf{y},0)\left[(\nabla h_{1,2}(\mathbf{x}))^2 + (\nabla h_{1,2}(\mathbf{y}))^2\right] \\ &+\frac{1}{2}\partial_z^2 G^d(\mathbf{x}-\mathbf{y},0)[h_{1,2}(\mathbf{y}) - h_{1,2}(\mathbf{x})]^2\Big\}. \end{aligned}$$

The matrix M_0 is diagonal in Fourier space and can be easily inverted as

$$M_0^{-1}(\mathbf{p},\mathbf{q}) = \frac{1}{\mathcal{N}(\mathbf{p})}\begin{bmatrix} G^d(\mathbf{p}) & -G^d(\mathbf{p},H) \\ -G^d(\mathbf{p},H) & G^d(\mathbf{p}) \end{bmatrix} (2\pi)^D\delta^D(\mathbf{p}+\mathbf{q}). \tag{B5}$$

We then calculate $\ln \mathcal{Z}_h = -\frac{1}{2}\,\mathrm{tr}\ln(1+M_0^{-1}\delta M)$, using the expansion of the logarithm up to the second order. We also choose $\int \mathrm{d}^D\mathbf{x}\; h(\mathbf{x}) = 0$ without loss of generality, leading to

$$\begin{aligned}
\ln \mathcal{Z}_h = -\frac{1}{2}\int \frac{\mathrm{d}^D\mathbf{p}}{(2\pi)^D}\int \mathrm{d}^D\mathbf{x}\mathrm{d}^D\mathbf{y}\Bigg\{ & \frac{G^d(\mathbf{p})}{\mathcal{N}(\mathbf{p})}\,\mathrm{e}^{i\mathbf{p}\cdot(\mathbf{x}-\mathbf{y})}\Big[G^d(\mathbf{x}-\mathbf{y},0)\left((\nabla h_1(\mathbf{x}))^2+(\nabla h_2(\mathbf{x}))^2\right) \\
& +\frac{1}{2}\partial_z^2 G^d(\mathbf{x}-\mathbf{y},0)\left((h_1(\mathbf{y})-h_1(\mathbf{x}))^2+(h_2(\mathbf{y})-h_2(\mathbf{x}))^2\right)\Big] \\
& -\frac{G^d(\mathbf{p},H)}{\mathcal{N}(\mathbf{p})}\,\mathrm{e}^{i\mathbf{p}\cdot(\mathbf{x}-\mathbf{y})}\Big[G^d(\mathbf{x}-\mathbf{y},H)\left((\nabla h_1(\mathbf{x}))^2+(\nabla h_2(\mathbf{x}))^2\right) \\
& +\partial_z^2 G^d(\mathbf{x}-\mathbf{y},H)\left(h_2(\mathbf{y})-h_1(\mathbf{x})\right)^2\Big]\Bigg\} \\
+\frac{1}{2}\int \frac{\mathrm{d}^D\mathbf{p}}{(2\pi)^D}\frac{\mathrm{d}^D\mathbf{q}}{(2\pi)^D} & \left(\frac{G^d(\mathbf{p})G^d(\mathbf{q})+G^d(\mathbf{p},H)G^d(\mathbf{q},H)}{\mathcal{N}(\mathbf{p})\mathcal{N}(\mathbf{p})}\right) \\
\times & \left\{\int \mathrm{d}^D\mathbf{x}\mathrm{d}^D\mathbf{v}\;\mathrm{e}^{i\mathbf{q}\cdot\mathbf{x}+i\mathbf{p}\cdot\mathbf{v}}\;\partial_z G^d(\mathbf{v}-\mathbf{x},H)h_2(\mathbf{x}) - \int \mathrm{d}^D\mathbf{x}\mathrm{d}^D\mathbf{v}\;\mathrm{e}^{i\mathbf{p}\cdot\mathbf{x}+i\mathbf{q}\cdot\mathbf{v}}\;\partial_z G^d(\mathbf{v}-\mathbf{x},H)h_1(\mathbf{x})\right\} \\
\times & \left\{\int \mathrm{d}^D\mathbf{y}\mathrm{d}^D\mathbf{u}\;\mathrm{e}^{-i\mathbf{q}\cdot\mathbf{y}-i\mathbf{p}\cdot\mathbf{u}}\;\partial_z G^d(\mathbf{u}-\mathbf{y},H)h_2(\mathbf{y}) - \int \mathrm{d}^D\mathbf{y}\mathrm{d}^D\mathbf{u}\;\mathrm{e}^{-i\mathbf{p}\cdot\mathbf{y}-i\mathbf{q}\cdot\mathbf{u}}\;\partial_z G^d(\mathbf{u}-\mathbf{y},H)h_1(\mathbf{y})\right\}.
\end{aligned} \tag{B6}$$

Integration over $\mathbf{u}-\mathbf{y}$ and $\mathbf{v}-\mathbf{x}$ can now be performed followed by integrations over $\mathbf{p}$ and $\mathbf{q}$, resulting in Eq.(14). Note that we have eliminated some uninteresting terms that were proportional to $\int d^D\mathbf{p}$ and $\int d^D\mathbf{p}\;\mathbf{p}^2$. Such integrals are usually removed in the framework of dimensional regularization [36], and don't play any important role. They appear since the "constant" infinite energy that is usually neglected when quantizing a field, now depends on the configuration of the surfaces. When we dynamically deform the boundaries, this contribution changes. These terms give rise to cut-off corrections to mass and surface tension as discussed in Ref. [19]

[1] H.B.G. Casimir, Proc. K. Ned. Akad. Wet. **51**, 793 (1948).
[2] V.M. Mostepanenko and N.N. Trunov, Sov. Phys. Usp. **31**, 965 (1988).
[3] P.W. Milloni, *The Quantum Vacuum* (Academic Press, New York, 1994).
[4] M. Krech, *The Casimir effect in critical systems* (World Scientific, Singapore, 1994).
[5] M. Kardar and R. Golestanian, submitted to Rev. Mod. Phys. (Colloquia)(1997).
[6] S.K. Lamoreaux, Phys. Rev. Lett. **78**, 5 (1997).
[7] R. Balian and B. Duplantier, Ann. Phys. (N.Y.)**112**, 165 (1978).
[8] H. Li and M. Kardar, Phys. Rev. Lett. **67**, 3275 (1991); Phys. Rev. A **46**, 6490 (1992).
[9] M. Bordag, G.L. Klimchitskaya, V.M. Mostepanenko, Phys. Lett. A **200**, 95 (1995).
[10] G.T. Moore, J. Math. Phys. **11**, 2679 (1970).
[11] S.A. Fulling, and P.C.W. Davies, Proc. R. Soc. A **348**, 393 (1976).
[12] M.-T. Jaekel, and S. Reynaud, Phys. Lett. A **167**, 227 (1992).
[13] P.A. Maia Neto, and S. Reynaud, Phys. Rev. A **47**, 1639 (1993).
[14] P.A. Maia Neto and L.A.S. Machado, Braz. J. Phys. **25**, 324 (1995).
[15] G. Calucci, J. Phys. A: Math. Gen. **25**, 3873 (1992); C.K. Law, Phys. Rev. A **49**, 433 (1994); V.V. Dodonov, Phys. Lett. A **207**, 126 (1995).
[16] O. Meplan and C. Gignoux, Phys. Rev. Lett. **76**, 408 (1996).
[17] A. Lambrecht, M.-T. Jaekel, and S. Reynaud, Phys. Rev. Lett. **77**, 615 (1996).
[18] P. Davis, Nature **382**, 761 (1996).
[19] L.H. Ford and A. Vilenkin, Phys. Rev. D **25**, 2569 (1982).
[20] The calculated force also has causality problems reminiscent of the radiation reaction forces in classical electron theory. However, it has been shown that this problem, which is an artifact of the unphysical assumption of perfect reflectivity of

the mirror at any frequency, can be resolved by taking frequency dependent reflectivity and transmittivity functions that respect the Kramers–Kronig relations [12].
[21] C. Eberlein, Phys. Rev. Lett. **76**, 3842 (1996); Phys. Rev. A **53**, 2772 (1996).
[22] P. Knight, Nature **381**, 736 (1996).
[23] G. Barton and C. Eberlein, Ann. Phys. (N.Y.) **227**, 222 (1993).
[24] V.V. Dodonov, A.B. Klimov, and V.I. Man'ko, Phys. Lett. A **142**, 511 (1989).
[25] L.S. Levitov, Europhys. Lett. **8**, 499 (1989).
[26] V.E. Mkrtchian, Phys. Lett. A **207**, 299 (1995).
[27] J.B. Pendry, preprint (1997) cond-mat/9707190.
[28] V.V. Dodonov, Phys. Lett. A **207**, 126 (1995).
[29] See Appendix B for the differences between the present formalism and that of Ref. [8].
[30] This identification of the effective mass is based simply on the naive use of a Newtonian equation of motion for the plate. This is criticized in Ref. [12], as the equation of motion is in fact more complicated, involving also higher time derivatives. However, our usage of the term is in line with other examples, such as the effective mass of an electron in a crystal.
[31] R. Golestanian, M. Goulian, and M. Kardar, Europhys. Lett. **33**, 241 (1996); Phys. Rev. E **54**, 6725 (1996).
[32] P.A. Maia Neto, private communication.
[33] J. D. Joannopoulos, R. D. Meade, and J. N. Winn, *Photonic Crystals* (Princeton University Press, Princeton, 1995).
[34] L.D. Landau and E.M. Lifshitz, *The classical theory of fields* (Pergamon Press, England, fourth edition, 1975).
[35] S.J. Chang, *Introduction to quantum field theory* (World Scientific, Singapore, 1990).
[36] J. Zinn-Justin, *Quantum field theory and critical phenomena* (Oxford University Press, England, second edition, 1993).

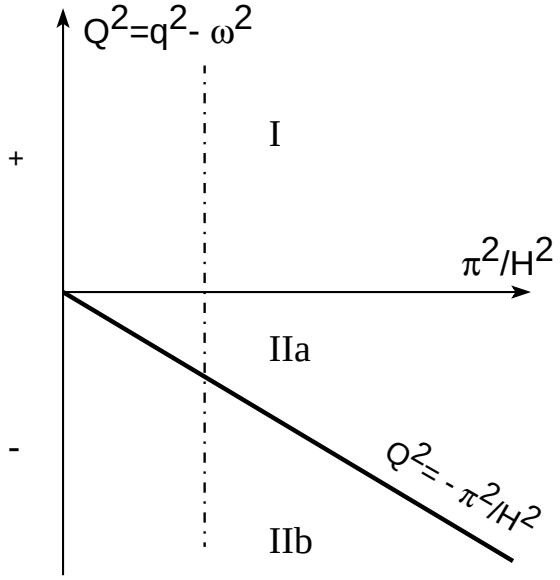

FIG. 1. Different regions of the $(\mathbf{q}, \omega)$ plane.